NANO LETTERS
Letter
Cite This: Nano Lett. 2017, 17, 7839−7846
pubs.acs.org/NanoLett

Porous-Shell Vanadium Nitride Nanobubbles with Ultrahigh Areal Sulfur Loading for High-Capacity and Long-Life Lithium−Sulfur Batteries

Lianbo Ma,[†] Hao Yuan,[†] Wenjun Zhang,[†] Guoyin Zhu,[†] Yanrong Wang,[†] Yi Hu,[†] Peiyang Zhao,[†] Renpeng Chen,[†] Tao Chen,[†] Jie Liu,[†,‡] Zheng Hu,[†] and Zhong Jin*[,†]

[†]Key Laboratory of Mesoscopic Chemistry of MOE, School of Chemistry and Chemical Engineering, Nanjing University, Nanjing, Jiangsu 210023, China

[‡]Department of Chemistry, Duke University, Durham, North Carolina 27708, United States

Supporting Information

ABSTRACT: Lithium−sulfur (Li−S) batteries hold great promise for the applications of high energy density storage. However, the performances of Li−S batteries are restricted by the low electrical conductivity of sulfur and shuttle effect of intermediate polysulfides. Moreover, the areal loading weights of sulfur in previous studies are usually low (around 1−3 mg cm^{-2}) and thus cannot fulfill the requirement for practical deployment. Herein, we report that porous-shell vanadium nitride nanobubbles (VN-NBs) can serve as an efficient sulfur host in Li−S batteries, exhibiting remarkable electrochemical performances even with ultrahigh areal sulfur loading weights (5.4−6.8 mg cm^{-2}). The large inner space of VN-NBs can afford a high sulfur content and accommodate the volume expansion, and the high electrical conductivity of VN-NBs ensures the effective utilization and fast redox kinetics of polysulfides. Moreover, VN-NBs present strong chemical affinity/adsorption with polysulfides and thus can efficiently suppress the shuttle effect via both capillary confinement and chemical binding, and promote the fast conversion of polysulfides. Benefiting from the above merits, the Li−S batteries based on sulfur-filled VN-NBs cathodes with 5.4 mg cm^{-2} sulfur exhibit impressively high areal/specific capacity (5.81 mAh cm^{-2}), superior rate capability (632 mAh g^{-1} at 5.0 C), and long cycling stability.

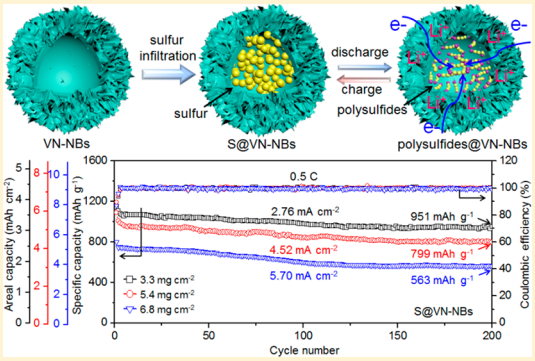

KEYWORDS: *Vanadium nitride, porous-shell nanobubbles, lithium−sulfur batteries, specific/areal capacity, suppression of shuttle effect*

In the past decades, rechargeable lithium-ion batteries (LIBs) have achieved great successes in the fields of portable electronics and clean-energy vehicles.[1,2] However, the energy density of LIBs is approaching a formidable limit; thus, it is hard to meet the rapidly growing demands. As a promising candidate for next-generation batteries, lithium−sulfur (Li−S) batteries have caught tremendous attention, owing to the high theoretical capacity (1675 mAh g^{-1}) and energy density (2600 Wh kg^{-1}).[3,4] The reserve abundance and nontoxicity of sulfur also bring attractive low cost and environmental friendless to Li−S batteries.[5] However, the development of practically reliable Li−S batteries is hindered by some critical problems, especially the easy dissolution of intermediate polysulfides,[6−9] which can result in reduced capacity, fast capacity degradation, and low Coulombic efficiency.[10−12] Furthermore, the poor conductivity of sulfur is inimical to rate capability and limits the utilization ratio and areal sulfur loading. To achieve a competitive specific capacity for the assembled battery packs, normally the areal loading mass of sulfur shall be higher than ∼5 mg cm^{-2}.[8] However, in the previous reports, the loading weights of sulfur are usually limited to about 1−3 mg cm^{-2}, and the further increase of sulfur loading cannot effectively improve the areal specific capacity and thus is not sufficient enough for practical use.

Strenuous efforts, as summarized in the review articles,[13−15] have been made to address the above issues, such as incorporating sulfur into the porous and conductive host materials,[16] developing novel electrolytes and additives,[17] and applying functional interlayers and binders.[18] With high conductivity and regulable porosity, carbon materials are the most studied sulfur hosts for constructing sulfur composite cathodes.[19] Nevertheless, the weak interactions between nonpolar carbon and charged sulfur species are not favorable to the confinement of sulfur.[20] In recent years, hollow nanostructures of polar materials with strong interactions with polysulfides have been regarded as alternative polysulfide adsorbent and physical barriers. In the pioneering works, porous transition metal compounds including TiO_x, MnO_2,

Received: September 21, 2017
Revised: November 17, 2017
Published: November 28, 2017

DOI: 10.1021/acs.nanolett.7b04084
Nano Lett. 2017, 17, 7839−7846

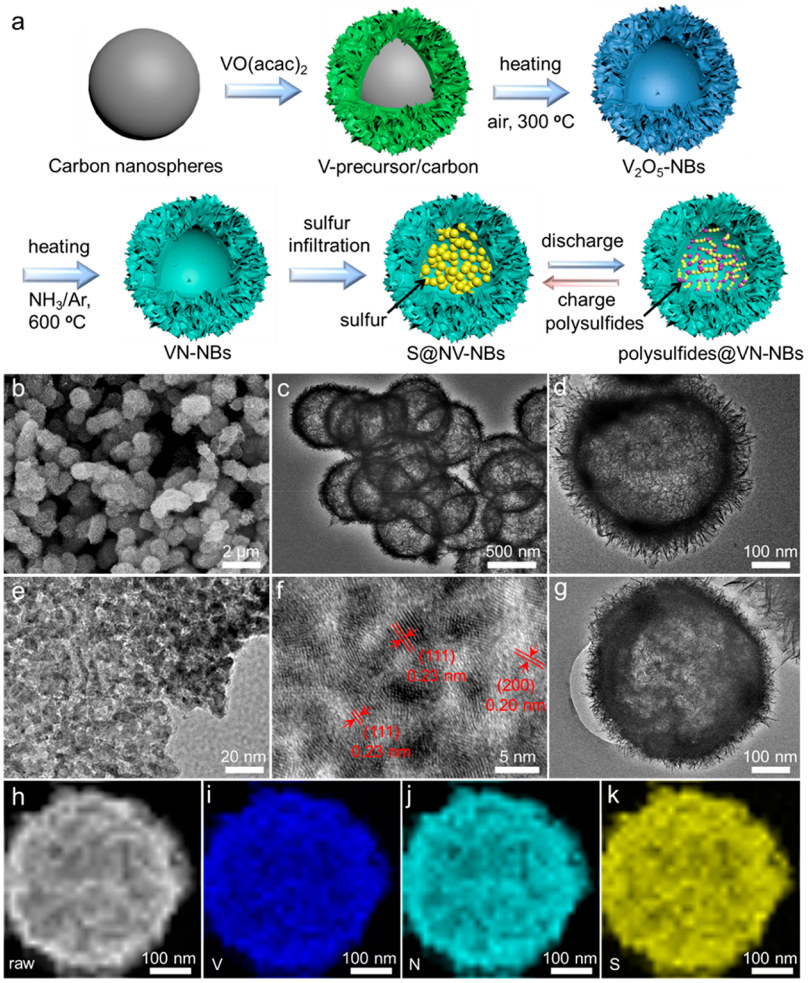

Figure 1. Synthesis and microscopic characterizations of the samples. (a) Schematic illustration of the synthesis of VN-NBs and S@VN-NBs composites. (b) SEM, (c–e) TEM, and (f) HRTEM images of VN-NBs. (g) TEM, (h) STEM, and (i–k) corresponding elemental mappings (V, N, and S elements) of S@VN-NBs composite.

TiN, CoS_x, and Co_4N have been reported to improve the polysulfide retention.[21−31] Nevertheless, the porosity and conductivity of inorganic compound nanostructures are contradictory and hard to be fully satisfied and thus may cause high charge transfer resistance and sluggish interfacial redox reaction kinetics, resulting in decreased sulfur utilization and rate capability. Therefore, it can be deduced that a promising polar material-based sulfur host should possess the following structural and compositional features: (1) large void space to store sulfur and accommodate the volume expansion; (2) strong affinity and adsorption ability with polysulfides to improve the sulfur retention;[27,28] (3) high electrical conductivity to ensure the sufficient utilization of sulfur and boost the interfacial redox reaction kinetics; and (4) electrocatalytic effects for sulfur redox reactions to promote the fast conversion of sulfur species.[23]

Herein, we report that porous-shell vanadium nitride nanobubbles (VN-NBs) can simultaneously meet the demands of a superb sulfur host material for cathodes in Li−S batteries. Notably, VN has a remarkable electrical conductivity of $\sim 10^6$ S·m^{-1} at room temperature.[32] With the intriguing high-porosity hollow structure, strong polarity and chemical adsorption ability for polysulfides, high electrical conductivity, and catalytic effect for fast sulfur conversion, the cathodes based on sulfur-encapsulated VN-NBs (S@VN-NBs) exhibit remarkable electrochemical performances in Li−S batteries. Impressively, the S@VN-NBs cathodes with high areal sulfur loadings can deliver very high specific/areal capacity along with long cycling life, which is remarkable among the existing sulfur cathodes based on metallic compound nanostructures (Table S1).[21−31,33−39]

To controllably prepare the VN-NBs with porous-shell hollow structure (Figure 1a), a two-step organometallic compound conversion and thermal nitridation process was developed, as detailed in the Experimental Section of the Supporting Information. Uniform monodispersed carbon nanospheres (~500 nm) were used as the sacrifice template (Figure S1). First, vanadium-based precursor was homogeneously capped on the surface of carbon nanospheres. Then, carbon nanospheres were removed by heating under air, and vanadium species were simultaneously converted into V_2O_5 nanobubbles (V_2O_5−NBs), as confirmed by X-ray diffraction (XRD) analysis in Figure S2. Finally, V_2O_5−NBs were further treated under NH_3/Ar atmosphere, resulting in the formation of VN-NBs with porous shells and interior void spaces. For the encapsulation of sulfur in the hollow nanobubbles, high purity sulfur was infiltrated into VN-NBs through a melt-diffusion strategy.[40,41] As schematically illustrated in Figure 1a, elemental sulfur can be completely absorbed into the interior space of VN-NBs through capillary action, enabling a high sulfur

DOI: 10.1021/acs.nanolett.7b04084
Nano Lett. 2017, 17, 7839−7846

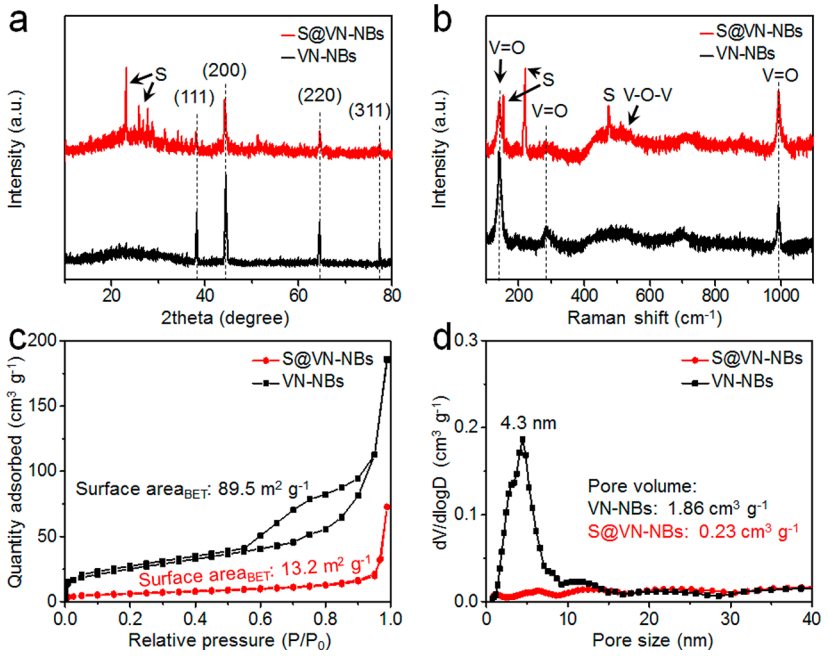

Figure 2. Structural characterizations of VN-NBs and S@VN-NBs. (a) XRD patterns, (b) Raman spectra, (c) N_2 adsorption/desorption isotherms, and (d) pore size distribution curves of VN-NBs and S@VN-NBs.

percentage. During the charge/discharge processes, VN-NBs also act as the efficient host for the conversion and containment of lithium polysulfides. The hollow nanostructure and strong adsorption ability of VN-NBs can synergistically restrict the polysulfide shuttle effects via physical and chemical ways, and bring a favorable electrocatalytic effect that enables the rapid redox reaction kinetics of polysulfides.

Figure 1b shows a scanning electron microscopy (SEM) image of as-prepared VN-NBs, revealing the homogeneous distributed hollow spherical structure of approximately 500 nm in diameter and the hierarchical porous surface. The nanobubbles show almost no structural collapse, indicating the high structural integrity even after high-temperature treatment. Transmission electron microscopy (TEM) reveals the large interior hollow spaces in VN-NBs, and the average thickness of porous shells is measured to be 50 nm (Figure 1c,d). The highly porous walls of VN-NBs consist of closely interconnected ultrathin nanosheets (Figure 1e), which are mainly aggregated and fused by numerous VN nanoparticles with about 3−5 nm in size (Figure 1f). High-resolution TEM (HRTEM) image in Figure 1f displays two different lattice distances of 0.23 and 0.20 nm, attributing to the (111) and (200) planes of VN, respectively.

After the filling of sulfur into VN-NBs, the morphology and compositions of resultant S@VN-NBs composite were also examined. Figure S3 presents the SEM images of S@VN-NBs at different magnifications. Clearly, S@VN-NBs maintains the initial morphology of VN-NBs, and no sulfur particles are observed on the surface. Moreover, the S@VN-NBs presents much darker contrast (Figure 1g), which mainly resulted from the encapsulation of sulfur inside VN-NBs. To illustrate the spatial distributions of component elements, scanning TEM (STEM) and elemental mappings were conducted (Figure 1h−k). The detected elements include V, N, and S elements, and the elemental mappings confirm their homogeneous distributions in VN-NBs. Notably, the elemental mapping in Figure 1k reveals the preservation of S element absorbed in the porous shells of VN-NBs even after thermal treatment, owing to the strong adsorption capability of VN-NBs to sulfur.

The compositions and crystalline of VN-NBs and S@VN-NBs products were examined by XRD and Raman spectroscopy. As shown in Figure 2a, both VN-NBs and S@VN-NBs exhibit the typical XRD peaks belonging to cubic VN (JCPDS card, No. 25−1252). Additionally, the S@VN-NBs sample displays the diffraction peaks of elemental sulfur, confirming the existence of sulfur in the composite. The structural features of VN-NBs and S@VN-NBs products were further investigated by Raman spectroscopy (Figure 2b). In additional to the characteristics of VN,[32] the Raman spectrum of S@VN-NBs also shows the presence of elemental sulfur.

The specific surface area and pore size characteristics of VN-NBs and S@VN-NBs were investigated by N_2 adsorption/desorption isotherms. As illustrated in Figure 2c, the isotherms of VN-NBs disclose the typical II model, and the specific surface area of VN-NBs calculated by Brunauer−Emmett−Teller (BET) method is 89.5 $m^2\ g^{-1}$, with a corresponding pore volume of 1.86 $cm^3\ g^{-1}$. The pore size distribution of VN-NBs was further analyzed in Figure 2d, revealing the abundant mesopores centered at 4.3 nm. After infiltrating sulfur into VN-NBs, the specific surface area and pore volume of S@VN-NBs decrease to 13.2 $m^2\ g^{-1}$ and 0.23 $cm^3\ g^{-1}$, respectively, owning to the sulfur occupation in the internal space.

The chemical states of VN-NBs and S@VN-NBs were examined by X-ray photoelectron spectroscopy (XPS). The survey XPS spectrum of VN-NBs in Figure S4 implies the coexistence of V and N elements. The high-resolution XPS spectrum at V $2p_{3/2}$ region in Figure S5a can be fitted into three peaks at 512.3, 513.5, and 515.6 eV, attributing to the V^0, V^{2+}, and V^{3+} species, respectively.[42,43] This result indicates the presence of a partial oxidation layer on the surface of VN-NBs.[44,45] The high-resolution XPS spectrum at the N 1s region (Figure S5b) exhibits the characteristic peak of metal nitride at 396.5 eV.[46] Another peak at around 399.1 eV is assigned to the nitrogen bonding to the oxide layer on the surface. As for S@

DOI: 10.1021/acs.nanolett.7b04084
Nano Lett. 2017, 17, 7839−7846

VN-NBs, besides the XPS signals of V and N elements, additional XPS signal belonging to S was also detected (Figure S6a). A pair of peaks at 165.0 and 163.9 eV, is observed at S 2p region (Figure S6b), confirming that the sulfur species entrapped in VN-NBs mainly existed in the forms of S_8 molecules.[47,48] The accurate loading content of sulfur in S@VN-NBs was determined by thermogravimetric analysis (TGA) under N_2 atmosphere heated from room temperature to 600 °C. As shown in Figure S7, the S@VN-NBs start to lose weight at around 200 °C, and the weight maintains stable after the temperature arises to 450 °C. The sulfur content in S@VN-NBs revealed by TGA is 78.2 wt %.

As a control sample, S@V_2O_5−NBs was also prepared by skipping the thermal nitridation step. The SEM and TEM characterizations (Figure S8a,b) show the spherical morphology and interior hollow structure of V_2O_5−NBs, similar to the VN-NBs. The Raman spectrum of V_2O_5−NBs in Figure S9a reveals the typical Raman characteristics of V_2O_5.[49] After filling sulfur into V_2O_5−NBs, the elemental mappings of S@V_2O_5−NBs (Figure S8c−f) suggest the coexistence of V, O, and S elements and demonstrate their homogeneous distributions. Additionally, the TGA curve in Figure S9b indicates that the accurate sulfur content of S@V_2O_5−NBs is 74.1 wt %.

To demonstrate the strong affinity between VN-NBs and sulfur species, theoretical simulation based on density functional theory (DFT) method was conducted to evaluate the binding energies between these components. The (200) plane of VN was selected as the interacted surface because of its stable state. As indicated in Figure 3a, the binding energies between the (200) plane of VN with Li_2S, Li_2S_2, Li_2S_4, Li_2S_6, Li_2S_8, and S_8 species are calculated to be −3.86, −3.14, −3.27, −3.01, −3.46, and −2.21 eV, respectively. These values are much higher than those of V_2O_5 (Figure S10) and graphitic carbon,[50] suggesting the strong interactions between VN and sulfur species. Moreover, to experimentally confirm the strong absorption of VN-NBs with sulfur species, a visual observation was conducted by adding VN-NBs or V_2O_5-NBs into a solution of 0.05 M Li_2S_6 in mixed dioxolane/dimethoxyethane (DOL/DME, 1:1 in volume). As shown in Figure 3b, after the adding of VN-NBs for 15 min, the color of Li_2S_6 solution becomes lighter and turns almost colorless after 30 min. While for V_2O_5−NBs (Figure S11), the Li_2S_6 solution turns almost colorless after about 45 min. This further indicates the stronger adsorption ability of VN-NBs with sulfur species, consistent well with the theoretical simulation.

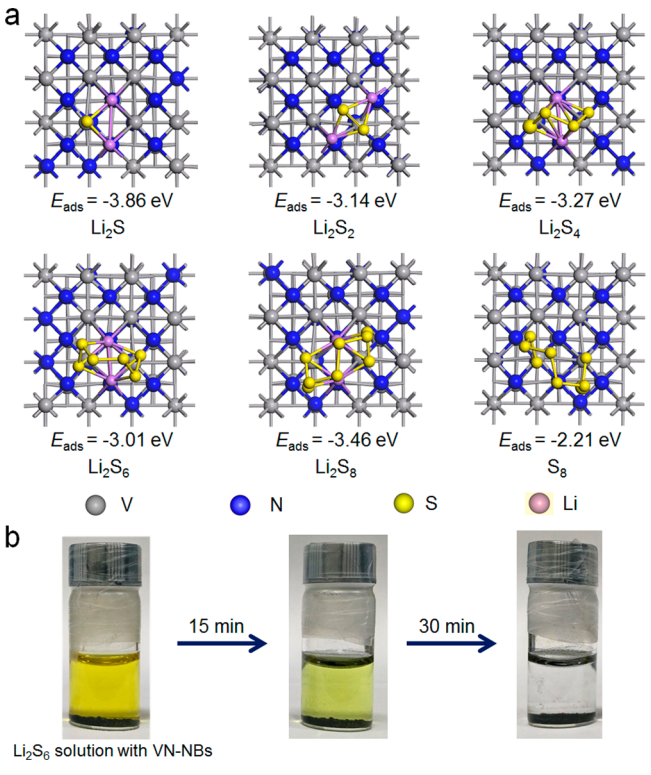

Figure 3. Theoretical simulation and experimental testing of the polysulfide adsorption ability of VN-NBs. (a) Binding geometric configurations and binding energies of sulfur species with the (200) plane of VN. The high binding energies indicate the strong adsorption of VN with sulfur species. (b) Adsorption ability tests of VN-NBs with Li_2S_6 as a representative lithium polysulfide.

The electrochemical properties of S@VN-NBs as sulfur cathode for Li−S batteries were evaluated systematically. Figure 4a presents the cyclic voltammetry (CV) curves of S@VN-NBs cathode with the sulfur loading weight of 1.2 mg cm^{-2} at a scanning rate of 0.2 mV s^{-1}.[33] Two cathodic peaks and one anodic peak can be identified in the CV curve of the initial cycle. The cathodic peaks at 2.28 and 2.03 V are attributed to the formation of long-chain soluble polysulfides (Li_2S_x, $4 < x \leq 8$) from S_8, and subsequently the formation of short-chain insoluble sulfides (Li_2S_2 and Li_2S), respectively. The single anodic peak at 2.39 V is assigned to the reverse conversion of short-chain sulfides to S_8.[51,52] From the second cycle onward, the peak positions of CV curves kept almost stable as compared to those of the initial cycle, implying the good cycling stability of S@VN-NBs cathode. Figure S12a compares the initial CV curves of S@VN-NBs cathode with S@V_2O_5-NBs cathode. The CV curve of S@VN-NBs cathode shows apparent positive shift in the reduction peaks, negative shift in the oxidation peak, and higher peak current densities as compared with those of S@V_2O_5−NBs cathode. Moreover, the electrocatalytic effect of VN-NBs was confirmed by the changes in onset potentials for all three redox peaks. The onset potentials were taken at a current density of 10 μA cm^{-2} beyond the baseline current, following a common definition employed in electrocatalysis.[53] As shown in Figure S13, compared with V_2O_5−NBs, the VN-NBs show increased onset potentials of cathodic peaks and decreased onset potentials of anodic peaks, implying an accelerated kinetics promoted by the electrocatalytic effect of VN-NBs.[53]

Figure 4b displays the galvanostatic charge/discharge profiles of S@VN-NBs cathodes under the current rates ranged from 0.2 to 5.0 C (1.0 C = 1675 mA g^{-1}). All the charge/discharge profiles exhibit two discharge plateaus at around 2.37 and 2.10 V and one large charge plateau between 2.2 and 2.4 V, which are consistent with those of CV results. Moreover, at 0.2 C, the initial discharge capacity reaches 1536 mAh g^{-1}, suggesting the efficient utilization of sulfur. When the current rate increases from 0.2 to 0.5, 1.0, 2.0, and 5.0 C, the charge/discharge profiles still retain the typical features of elemental sulfur, suggesting that the S@VN-NBs cathodes work well under high rates, and the conversion between S_8 and Li_2S_x is highly thorough and reversible. Additionally, Figure S12b shows the galvanostatic charge/discharge profiles of S@VN-NBs and S@V_2O_5-NBs cathodes at 0.2 C. Compared to the S@V_2O_5−NBs cathode, the S@VN-NBs cathode shows longer and more stable charge/discharge profile plateaus with smaller potential

DOI: 10.1021/acs.nanolett.7b04084
Nano Lett. 2017, 17, 7839−7846

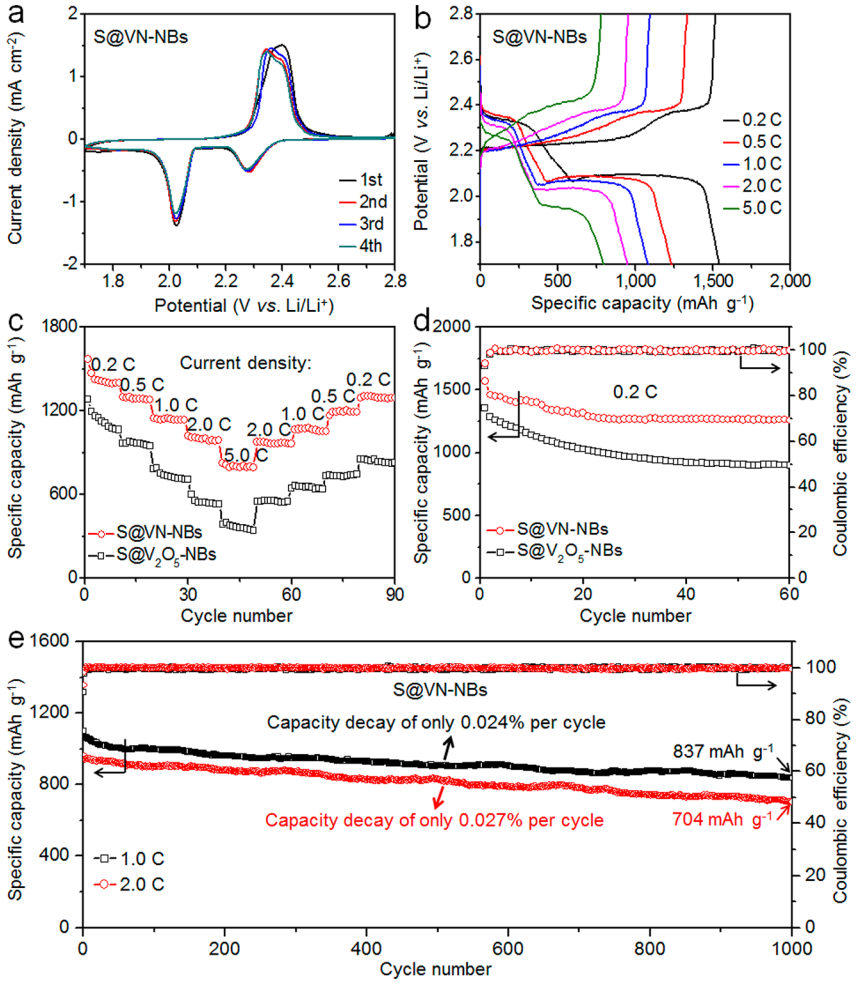

Figure 4. Electrochemical performances of S@VN-NBs and S@V_2O_5-NBs cathodes in Li−S batteries with the sulfur loading of 1.2 mg cm^{-2}. (a) CV curves of S@VN-NBs cathode at 0.2 mV s^{-1}. (b) Galvanostatic charge/discharge profiles of S@VN-NBs cathode under various current rates. (c) Rate capabilities and (d) cycling performances and Coulombic efficiencies of S@VN-NBs and S@V_2O_5-NBs cathodes. (e) Long-term cycling performances and corresponding Coulombic efficiencies of S@VN-NBs cathodes under 1.0 and 2.0 C.

polarizations, further indicating the more efficient reaction kinetics promoted by VN-NBs.[54]

Figure 4c compares the rate performances of S@VN-NBs and S@V_2O_5-NBs cathodes under various current rates from 0.2 to 5.0 C. Both cathodes show good rate performance, and the rate capability of S@VN-NBs cathode is even more superior. In detail, under 0.2, 0.5, 1.0, 2.0, and 5.0 C, the discharge capacities of S@VN-NBs cathode are 1428, 1294, 1142, 1008, and 812 mAh g^{-1}, respectively; while for the S@V_2O_5-NBs cathode, the corresponding discharge capacities decrease to 1156, 971, 746, 556, and 383 mAh g^{-1}, respectively. When the current rate returns to 0.2 C, the discharge capacities of S@VN-NBs and S@V_2O_5-NBs cathodes recover to 1306 and 849 mAh g^{-1}, respectively. To figure out the charge transfer characteristics of S@VN-NBs and S@V_2O_5-NBs cathodes behind the outstanding rate performance, electrochemical impedance spectroscopy (EIS) was conducted (Figure S14). Owing to the dramatically enhanced electrical conductivity, the S@VN-NBs cathode exhibits much lower charge-transfer resistance compared to that of S@V_2O_5−NBs cathode, thus conducive to the rate capability.

From a practical perspective, the high cycling stability under both low and high current rates is critically important for Li−S batteries. Figure 4d presents the cycling performances of S@VN-NBs and S@V_2O_5-NBs cathodes under 0.2 C within the first 60 cycles. The S@VN-NBs cathode delivers an initial discharge capacity of 1568 mAh g^{-1} under 0.2 C, and it is able to maintain a stable cycling performance for 60 cycles (1258 mAh g^{-1}). Moreover, the Coulombic efficiency of S@VN-NBs cathode after 60 cycles is close to 100%. In comparison, the S@V_2O_5-NBs cathode displays lower discharge capacity (901 mAh g^{-1}) and comparable Coulombic efficiency after 60 cycles. To better illustrate the efficient utilization of sulfur in S@VN-NBs cathode, the VN-NBs (without the filling of sulfur) was tested as the cathode material for LIBs within 1.7 to 2.8 V vs. Li/Li^+ (Figure S15). It confirms that the lithium storage capacity of pristine VN-NBs without sulfur is very low and thus has very little contribution to the total discharge capacity of Li−S batteries. As the current rate increases to 1.0 and 2.0 C, the S@VN-NBs cathode still exhibits excellent cycling performance. As shown in Figure 4e, the initial discharge capacity of S@VN-NBs cathode at 1.0 C is 1100 mAh g^{-1}, and with the great capability to restrict polysulfide dissolution, the discharge capacity keeps very stable and maintains at 837 mAh g^{-1} after cycling 1000 cycles, accompanying with an average capacity decay per cycle of only 0.024%. In contrast, the S@V_2O_5-NBs cathode (Figure S16) shows inferior cycling performance, delivering lower discharge capacities (415 mAh g^{-1} after 1000 cycles under 1.0

DOI: 10.1021/acs.nanolett.7b04084
Nano Lett. 2017, 17, 7839−7846

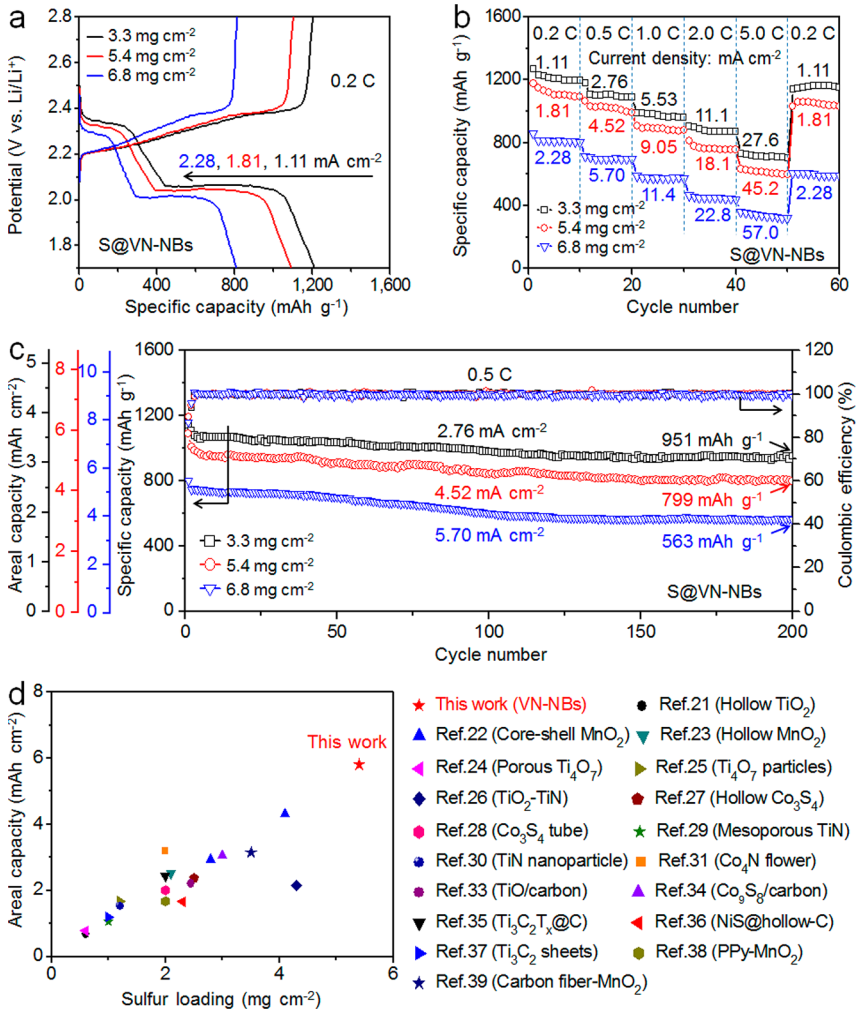

Figure 5. Electrochemical performances of S@VN-NBs cathodes with high areal loading weights of sulfur. (a) Galvanostatic charge/discharge profiles, (b) rate performances, and (c) long-term cycling capabilities of S@VN-NBs cathodes with sulfur loading of 3.3, 5.4, and 6.8 mg cm^{-2}, respectively. (d) Areal capacity of S@VN-NBs cathode with sulfur loading of 5.4 mg cm^{-2} at 0.5 C compared with other previously reported sulfur host materials in the literatures.

C with an overall capacity retention of 46.5%). Moreover, the Coulombic efficiencies of S@VN-NBs cathode within the 1000 cycles are above 99.5%, indicating that the VN-NBs can effectively suppress the dissolution of polysulfides into organic-based electrolyte.[55] Figure S17 shows the EIS spectra of S@VN-NBs and S@V_2O_5-NBs cathodes after cycling for 1000 times at 1.0 C. Clearly, the S@VN-NBs cathode after long-term cycling shows significantly reduced charge-transfer resistance compared with that before cycling; while the S@V_2O_5-NBs cathode after cycling exhibits slightly reduced charge-transfer resistance. These results further confirm the high electrical conductivity and low impedance of VN-NBs. Even under 2.0 C, the S@VN-NBs cathode also displays outstanding cycling performance with high Coulombic efficiencies above 99.0%. The initial discharge capacity of S@VN-NBs cathode at 2.0 C is 960 mAh g^{-1}, and it retains a high discharge capacity of 704 mAh g^{-1} after 1000 cycles. This corresponds to a capacity retention of 73.3% relative to the initial cycle, and the capacity loss is as low as 0.027% per cycle. Figure S18 shows the SEM image of S@VN-NBs after 1000 cycles at 2.0 C. It can be seen that the S@VN-NBs after long-term cycling still maintain the original nanobubble morphology, suggesting the high structural integrity of VN-NBs. Compared with other VN-based sulfur cathodes in the literature,[56−59] the S@VN-NBs cathode exhibits remarkable electrochemical performances. Considering the structural differences of these VN-based nanostructures, the greatly enhanced electrochemical performances of VN-NBs in this work should be mainly attributed to the unique hierarchical porous shell and interior hollow structures of VN-NBs. Furthermore, compared with the typical sulfur cathodes based on inorganic nanostructures that are summarized in Table S1,[21−31,33−39] the S@VN-NBs cathode also demonstrates remarkable electrochemical performances, suggesting its good potential for future applications.

In consideration of the requirements for commercialization and scale-up fabrication, the S@VN-NBs cathodes with higher areal sulfur loading weights and large thicknesses were also prepared. The galvanostatic charge/discharge profiles of S@VN-NBs cathodes with the areal sulfur loading of 3.3, 5.4, and 6.8 mg cm^{-2} at 0.2 C (corresponding to 1.11, 1.81, and 2.28 mA cm^{-2}, respectively) exhibit the high discharge capacities of 1214, 1089, and 812 mAh g^{-1}, respectively (Figure 5a). Moreover, the cathodes display outstanding rate capabilities from 0.2 to 5.0 C (Figure 5b). The discharge capacities of S@VN-NBs cathode with areal sulfur loading of 3.3 mg cm^{-2} at 0.2, 0.5, 1.0, 2.0, and 5.0 C (corresponding to 1.11, 2.76, 5.53,

DOI: 10.1021/acs.nanolett.7b04084
Nano Lett. 2017, 17, 7839−7846

11.1, and 27.6 mA cm^{-2}, respectively) are 1223, 1105, 988, 876, and 717 mAh g^{-1}, respectively. When the sulfur loading increases to 5.4 mg cm^{-2}, the discharge capacities under 0.2, 0.5, 1.0, 2.0, and 5.0 C (corresponding to 1.81, 4.52, 9.05, 18.1, and 45.2 mA cm^{-2}, respectively) still maintain at 1130, 1033, 896, 770, and 632 mAh g^{-1}, respectively. With an ultrahigh sulfur loading of 6.8 mg cm^{-2}, the discharge capacities at 0.2, 0.5, 1.0, 2.0, and 5.0 C (corresponding to 2.28, 5.70, 11.4, 22.8, and 57.0 mA cm^{-2}, respectively) decrease to 818, 709, 589, 465, and 364 mAh g^{-1}, respectively. With the increase of areal sulfur loading, the specific capacity and rate performance of S@VN-NBs cathodes decrease gradually, which may result from the decreased interfacial conduction between electrolyte and electroactive sulfur components and the increased charge-transfer resistances (Figure S19).[8] Additionally, under 0.5 C, the S@VN-NBs cathodes with 3.3, 5.4, and 6.8 mg cm^{-2} sulfur, corresponding to 2.76, 4.52, and 5.70 mA cm^{-2}, respectively, exhibit the high initial discharge capacities of 1142, 1076, and 798 mAh g^{-1} (Figure 5c), respectively, corresponding to the areal specific capacities of 3.77, 5.81, and 5.43 mAh cm^{-2}, respectively. The areal specific capacity under 5.4 mg cm^{-2} sulfur loading reaches a peak value, which is remarkable among the existing sulfur cathode materials (Figure 5d and Table S1).[21−31,33−39] Moreover, the S@VN-NBs cathodes with high sulfur loading of 3.3, 5.4, and 6.8 mg cm^{-2} under 0.5 C show good cycling performances and deliver the discharge capacities of 951, 799, and 563 mAh g^{-1} after cycling for 200 cycles, respectively, and the corresponding capacity retentions are 83.2%, 74.3%, and 70.6% compared to the initial cycle. The outstanding performances of S@VN-NBs cathodes with high sulfur loadings are ascribed to the strong polysulfide absorption/confinement and high conductivity provided by VN-NBs, which facilitate the electron/ion transport and ensure the efficient sulfur utilization in the thick electrodes.

In summary, porous-shelled VN-NBs was found to be a promising sulfur host material for Li−S batteries. With the superior hollow structure, low charge transfer resistance, and strong chemical affinity for polysulfide trapping, the S@VN-NBs cathode can avoid the pervasive key issues of low electroactive sulfur utilization and severe shuttle effect in state-of-the-art Li−S batteries. Even under ultrahigh areal sulfur loadings of 5.4−6.8 mg cm^{-2}, the S@VN-NBs cathodes can exhibit stable cycling performances with remarkable specific/areal capacities, suggesting the significant potential of VN-NBs for use in battery packs. This study provides a feasible strategy for fabricating ordered nanostructural inorganic materials as efficient sulfur hosts in Li−S batteries.

■ ASSOCIATED CONTENT

Supporting Information

The Supporting Information is available free of charge on the ACS Publications website at DOI: 10.1021/acs.nanolett.7b04084.

Experimental section and supporting tables and figures (PDF)

■ AUTHOR INFORMATION

Corresponding Author

*E-mail: zhongjin@nju.edu.cn.

ORCID

Tao Chen: 0000-0003-2536-4145

Jie Liu: 0000-0003-0451-6111

Zheng Hu: 0000-0002-4847-899X

Zhong Jin: 0000-0001-8860-8579

Notes

The authors declare no competing financial interest.

■ ACKNOWLEDGMENTS

This work is supported by National Key Research and Development Program of China (2017YFA0208200, 2016YFB0700600, 2015CB659300), Projects of NSFC (21403105, 21573108), Natural Science Foundation of Jiangsu Province (BK20150583, BK20160647), and the Fundamental Research Funds for the Central Universities (020514380107).

■ REFERENCES

(1) Dunn, B.; Kamath, H.; Tarascon, J. M. *Science* **2011**, *334*, 928−935.

(2) Goodenough, J. B.; Park, K. S. *J. Am. Chem. Soc.* **2013**, *135*, 1167−1176.

(3) Bruce, P. G.; Freunberger, S. A.; Hardwick, L. J.; Tarascon, J. *Nat. Mater.* **2011**, *11*, 19−29.

(4) Evers, S.; Nazar, L. F. *Acc. Chem. Res.* **2013**, *46*, 1135−1143.

(5) Li, Z.; Wu, H. B.; Lou, X. W. D. *Energy Environ. Sci.* **2016**, *9*, 3061−3070.

(6) Zhang, J.; Hu, H.; Lou, X. W. *Angew. Chem., Int. Ed.* **2016**, *55*, 3982−3986.

(7) Yang, Y.; Zheng, G. Y.; Cui, Y. *Chem. Soc. Rev.* **2013**, *42*, 3018−3032.

(8) Peng, H. J.; Huang, J. Q.; Cheng, X. B.; Zhang, Q. *Adv. Energy Mater.* **2017**, *7*, 1700260.

(9) Lyu, Z. Y.; Xu, D.; Yang, L. J.; Che, R. C.; Feng, R.; Zhao, J.; Li, Y.; Wu, Q.; Wang, X. Z.; Hu, Z. *Nano Energy* **2015**, *12*, 657−665.

(10) Chung, S.; Manthiram, A. *Adv. Mater.* **2014**, *26*, 1360−1365.

(11) He, J.; Chen, Y.; Lv, W.; Wen, K.; Xu, C.; Zhang, W.; Li, Y.; Qin, W.; He, W. *ACS Nano* **2016**, *10*, 10981−10987.

(12) He, J.; Chen, Y.; Lv, W.; Wen, K.; Wang, Z.; Zhang, W.; Li, Y.; Qin, W.; He, W. *ACS Nano* **2016**, *10*, 8837−8842.

(13) Wild, M.; O'Neill, L.; Zhang, T.; Purkayastha, R.; Minton, G.; Marinescu, M.; Offer, G. J. *Energy Environ. Sci.* **2015**, *8*, 3477−3494.

(14) Rosenman, A.; Markevich, E.; Salitra, G.; Aurbach, D.; Garsuch, A.; Chesneau, F. F. *Adv. Energy Mater.* **2015**, *5*, 1500212.

(15) Eftekhari, A.; Kim, D. W. *J. Mater. Chem. A* **2017**, *5*, 17734−17776.

(16) Li, Z.; Guan, B. Y.; Zhang, J. T.; Lou, X. W. D. *Joule* **2017**, *1*, 576−587.

(17) Lin, Z.; Liu, Z.; Fu, W.; Dudney, N. J.; Liang, C. *Adv. Funct. Mater.* **2013**, *23*, 1064.

(18) Fan, Y.; Yang, Z.; Hua, W. X.; Liu, D.; Tao, T.; Rahman, M. M.; Lei, W. W.; Huang, S. M.; Chen, Y. *Adv. Energy Mater.* **2017**, *7*, 1602380.

(19) Wang, Q.; Yan, J.; Fan, Z. J. *Energy Environ. Sci.* **2016**, *9*, 729−762.

(20) Zhang, Q. F.; Wang, Y. P.; Seh, Z. W.; Fu, Z. H.; Zhang, R. F.; Cui, Y. *Nano Lett.* **2015**, *15*, 3780−3786.

(21) Seh, Z. W.; Li, W. Y.; Cha, J. J.; Zheng, G. Y.; Yang, Y.; McDowell, M. T.; Hsu, P. C.; Cui, Y. *Nat. Commun.* **2013**, *4*, 1331.

(22) Liang, X.; Nazar, L. F. *ACS Nano* **2016**, *10*, 4192−4198.

(23) Wang, X. L.; Li, G.; Li, J. D.; Zhang, Y. N.; Wook, A.; Yu, A. P.; Chen, Z. W. *Energy Environ. Sci.* **2016**, *9*, 2533−2538.

(24) Wei, H.; Rodrihuez, E. F.; Best, A. S.; Hollenkamp, A. F.; Chen, D. H.; Caruso, R. A. *Adv. Energy Mater.* **2017**, *7*, 1601616.

(25) Mei, S. L.; Jafta, C. J.; Lauermann, I. Q.; Ran, D.; Kargell, M.; Ballauff, M.; Lu, Y. *Adv. Funct. Mater.* **2017**, *27*, 1701176.

(26) Zhou, T.; Lv, W.; Li, J.; Zhou, G.; Zhao, Y.; Fan, S.; Liu, B.; Li, B.; Kang, F.; Yang, Q. H. *Energy Environ. Sci.* **2017**, *10*, 1694−1703.

(27) Xu, H. H.; Manthiram, A. *Nano Energy* **2017**, *33*, 124−129.

(28) Pu, J.; Shen, Z. H.; Zheng, J. X.; Wu, W. L.; Zhu, C.; Zhou, Q. W.; Zhang, H. G.; Pan, F. *Nano Energy* **2017**, *37*, 7−14.

DOI: 10.1021/acs.nanolett.7b04084
Nano Lett. 2017, 17, 7839−7846

(29) Cui, Z. M.; Zu, C. X.; Zhou, W. D.; Manthiram, A.; Goodenough, J. B. *Adv. Mater.* **2016**, *28*, 6926−6931.
(30) Hao, Z. X.; Yuan, L. X.; Chen, C. J.; Xiang, J. W.; Li, Y. Y.; Huang, Z. M.; Hu, P.; Huang, Y. H. *J. Mater. Chem. A* **2016**, *4*, 17711−17717.
(31) Deng, D. R.; Xue, F.; Jia, Y. J.; Ye, J. C.; Bai, C. D.; Zheng, M. S.; Dong, Q. F. *ACS Nano* **2017**, *11*, 6031−6039.
(32) Wang, R. T.; Lang, J. W.; Zhang, P.; Lin, Z. Y.; Yan, X. B. *Adv. Funct. Mater.* **2015**, *25*, 2270−2278.
(33) Li, Z.; Zhang, J. T.; Guan, B. Y.; Wang, D.; Liu, L. M.; Lou, X. W. *Nat. Commun.* **2016**, *7*, 13065.
(34) Chen, T.; Ma, L. B.; Cheng, B. R.; Chen, R. P.; Hu, Y.; Zhu, G. Y.; Wang, Y. R.; Liang, J.; Tie, Z. X.; Liu, J.; Jin, Z. *Nano Energy* **2017**, *38*, 239−248.
(35) Bao, W. Z.; Su, D. W.; Zhang, W. X.; Guo, X.; Wang, G. X. *Adv. Funct. Mater.* **2016**, *26*, 8746−8756.
(36) Ye, C.; Zhang, L.; Guo, C. X.; Li, D. D.; Vasileff, A.; Wang, H. H.; Qiao, S. Z. *Adv. Funct. Mater.* **2017**, *45*, 1702524.
(37) Liang, X.; Garsuch, A.; Nazar, L. F. *Angew. Chem., Int. Ed.* **2015**, *54*, 3907−3911.
(38) Zhang, J.; Shi, Y.; Ding, Y.; Zhang, W. K.; Yu, G. Y. *Nano Lett.* **2016**, *16*, 7276−7281.
(39) Li, Z.; Zhang, J. T.; Lou, X. W. *Angew. Chem., Int. Ed.* **2015**, *54*, 12886−12890.
(40) Chen, T.; Cheng, B. R.; Zhu, G. Y.; Chen, R. P.; Hu, Y.; Ma, L. B.; Lv, H. L.; Wang, Y. R.; Liang, J.; Tie, Z. X.; Jin, Z.; Liu, J. *Nano Lett.* **2017**, *17*, 437−444.
(41) Zheng, J. H.; Guo, G. N.; Li, H. W.; Wang, L.; Wang, B. W.; Yu, H. J.; Yan, Y. C.; Yang, D.; Dong, A. G. *ACS Energy Lett.* **2017**, *2*, 1105−1114.
(42) Wu, F.; Ye, Y. S.; Huang, J. Q.; Zhao, T.; Qian, J.; Zhao, Y. Y.; Li, L.; Wei, L.; Luo, R.; Huang, Y. X.; Xing, Y.; Chen, R. J. *ACS Nano* **2017**, *11*, 4694−4702.
(43) Zhou, X.; Shang, C.; Gu, L.; Dong, S.; Chen, X.; Han, P.; Li, L.; Yao, J.; Liu, Z.; Xu, H.; Zhu, Y.; Cui, G. *ACS Appl. Mater. Interfaces* **2011**, *3*, 3058−3063.
(44) Lu, X.; Liu, T.; Zhai, T.; Wang, G.; Yu, M.; Xie, S.; Ling, Y.; Liang, C.; Tong, Y.; Li, Y. *Adv. Energy Mater.* **2014**, *4*, 1300994.
(45) Yin, J.; Wang, L.; Tian, C.; Tan, T.; Mu, G.; Zhao, L.; Fu, H. *Chem. - Eur. J.* **2013**, *19*, 13979−13986.
(46) Glushenkov, A. M.; Hulicova-Jurcakova, D.; Llewellyn, D.; Lu, G. Q.; Chen, Y. *Chem. Mater.* **2010**, *22*, 914−921.
(47) Li, Z.; Yuan, L.; Yi, Z.; Sun, Y.; Liu, Y.; Jiang, Y.; Shen, Y.; Xin, Y.; Zhang, Z.; Huang, Y. *Adv. Energy Mater.* **2014**, *4*, 1301473.
(48) Mi, K.; Jiang, Y.; Feng, J.; Qian, Y.; Xiong, S. *Adv. Funct. Mater.* **2016**, *26*, 1571−1579.
(49) Ghimbeu, C. M.; Raymundo-Pinero, E.; Fioux, P.; Beguin, F.; Vix-Guterl, C. *J. Mater. Chem.* **2011**, *21*, 13268−13275.
(50) Ma, L. B.; Chen, R. P.; Zhu, G. Y.; Hu, Y.; Wang, Y. R.; Chen, T.; Liu, J.; Jin, Z. *ACS Nano* **2017**, *11*, 7274−7283.
(51) Li, G.; Sun, J.; Hou, W.; Jiang, S.; Huang, Y.; Geng, J. *Nat. Commun.* **2016**, *7*, 10601.
(52) Pei, F.; An, T.; Zang, J.; Zhao, X.; Fang, X.; Zheng, M.; Dong, Q.; Zheng, N. *Adv. Energy Mater.* **2016**, *6*, 1502539.
(53) Yuan, Z.; Peng, H. J.; Hou, T. Z.; Huang, J. Q.; Chen, C. M.; Wang, D. W.; Cheng, X. B.; Wei, F.; Zhang, Q. *Nano Lett.* **2016**, *16*, 519−527.
(54) Zhou, G. M.; Tian, H. Z.; Jin, Y.; Tao, X. Y.; Liu, B. F.; Zhang, R. F.; Seh, Z. W.; Zhuo, D.; Liu, Y. Y.; Sun, J.; Zhao, J.; Zu, C. X.; Wu, D. S.; Zhang, Q. F.; Cui, Y. *Proc. Natl. Acad. Sci. U. S. A.* **2017**, *114*, 840−845.
(55) Jia, J. X.; Wang, K.; Zhang, X.; Sun, X. Z.; Zhao, H. L.; Ma, Y. W. *Chem. Mater.* **2016**, *28*, 7864−7871.
(56) Sun, Z. H.; Zhang, J. Q.; Yin, L. C.; Hu, G. J.; Fang, R. P.; Cheng, H. M.; Li, F. *Nat. Commun.* **2017**, *8*, 14627.
(57) Li, X. X.; Ding, K.; Gao, B.; Li, Q. W.; Li, Y. Y.; Fu, J. J.; Zhang, X. M.; Chu, P. K.; Huo, K. F. *Nano Energy* **2017**, *40*, 655−662.
(58) Li, X. L.; Tang, R. W.; Hu, K.; Zhang, L. Y.; Ding, Z. Q. *Electrochim. Acta* **2016**, *210*, 734−742.
(59) Mosavati, N.; Salley, S. O.; Ng, K. Y. S. *J. Power Sources* **2017**, *340*, 210−216.

DOI: 10.1021/acs.nanolett.7b04084
Nano Lett. 2017, 17, 7839−7846